Authors for correspondence:
Berend Snel
e-mail: b.snel@uu.nl
Geert J. P. L. Kops
e-mail: g.kops@hubrecht.eu

THE ROYAL SOCIETY
PUBLISHING

Phylogenomics-guided discovery of a novel conserved cassette of short linear motifs in BubR1 essential for the spindle checkpoint

Eelco Tromer[1,4], Debora Bade[1], Berend Snel[4] and Geert J. P. L. Kops[1,2,3]

[1]Hubrecht Institute—KNAW (Royal Netherlands Academy of Arts and Sciences), Uppsalalaan 8, 3584 CT, Utrecht, The Netherlands
[2]Cancer Genomics Netherlands, and [3]Center for Molecular Medicine, University Medical Center Utrecht, 3584 CG, Utrecht, The Netherlands
[4]Theoretical Biology and Bioinformatics, Department of Biology, Science Faculty, Utrecht University, 3584 CH, Utrecht, The Netherlands

ET, 0000-0003-3540-7727; BS, 0000-0002-5804-8547; GJPLK, 0000-0003-3555-5295

The spindle assembly checkpoint (SAC) maintains genomic integrity by preventing progression of mitotic cell division until all chromosomes are stably attached to spindle microtubules. The SAC critically relies on the paralogues Bub1 and BubR1/Mad3, which integrate kinetochore–spindle attachment status with generation of the anaphase inhibitory complex MCC. We previously reported on the widespread occurrences of independent gene duplications of an ancestral 'MadBub' gene in eukaryotic evolution and the striking parallel subfunctionalization that lead to loss of kinase function in BubR1/Mad3-like paralogues. Here, we present an elaborate subfunctionalization analysis of the Bub1/BubR1 gene family and perform de novo sequence discovery in a comparative phylogenomics framework to trace the distribution of ancestral sequence features to extant paralogues throughout the eukaryotic tree of life. We show that known ancestral sequence features are consistently retained in the same functional paralogue: GLEBS/CMI/CDII/kinase in the Bub1-like and KEN1/KEN2/D-Box in the BubR1/Mad3-like. The recently described ABBA motif can be found in either or both paralogues. We however discovered two additional ABBA motifs that flank KEN2. This cassette of ABBA1-KEN2-ABBA2 forms a strictly conserved module in all ancestral and BubR1/Mad3-like proteins, suggestive of a specific and crucial SAC function. Indeed, deletion of the ABBA motifs in human BUBR1 abrogates the SAC and affects APC/C–Cdc20 interactions. Our detailed comparative genomics analyses thus enabled discovery of a conserved cassette of motifs essential for the SAC and shows how this approach can be used to uncover hitherto unrecognized functional protein features.

1. Introduction

Chromosome segregation during cell divisions in animals and fungi is monitored by a cell cycle checkpoint known as the spindle assembly checkpoint (SAC) [1–3]. The SAC couples absence of stable attachments between kinetochores and spindle microtubules to inhibition of anaphase by assembling a four-subunit inhibitor of the anaphase-promoting complex (APC/C), known as the MCC [4–6]. The molecular pathway that senses lack of attachment and produces the MCC relies on two related proteins known as Bub1 and BubR1/Mad3 [2]. Bub1 is a serine/threonine kinase that localizes to kinetochores and promotes recruitment of MCC subunits and of factors that stimulate its assembly [7–9]. These events are largely independent of Bub1 kinase activity, however, which instead is essential

for the correction process of attachment errors [7,10,11]. BubR1/Mad3 is one of the MCC subunits, responsible for directly preventing APC/C activity and anaphase onset [6,12,13]. It does so by contacting multiple molecules of the APC/C co-activator Cdc20, preventing APC/C substrate access and binding of the E2 enzyme UbcH10 [5,6,14,15]. The BubR1/Mad3–Cdc20 contacts occur via various short linear motifs (SLiMs) known as ABBA, KEN and D-box [6,9,14,16–20]. Like Bub1, BubR1 also impacts on the attachment error-correction process via a KARD motif that recruits the PP2A-B56 phosphatase [21–23]. This may not however be a universal feature of BubR1/Mad3-like proteins, because many lack a KARD-like motif.

Bub1 and BubR1/Mad3 are paralogues. We previously showed they originated by similar but independent gene duplications from an ancestral MadBub gene in many lineages, and that the two resulting gene copies then subfunctionalized in remarkably comparable ways [24]. An ancestral N-terminal KEN motif (KEN1: essential for the SAC) and an ancestral C-terminal kinase domain (essential for attachment error-correction) were retained in only one of the paralogous genes in a mutually exclusive manner in virtually all lineages (i.e. one gene retained KEN but lost kinase, while the other retained kinase but lost KEN). One exception to this 'rule' are vertebrates, where both paralogues have a kinase-like domain. The kinase domain of human BUBR1 however lacks enzymatic activity (i.e. is a pseudokinase) but instead confers stability onto the BUBR1 protein [24].

The similar subfunctionalization of Bub1 and BubR1/ Mad3-like paralogues was inferred from analysis of two domains (TPR and kinase) and one motif (KEN1). We set out to analyse whether any additional features specifically segregated to Bub1- or BubR1/Mad3-like proteins after duplications by designing an unbiased feature discovery pipeline and tracing feature evolution. The pipeline extracted all known and various previously unrecognized conserved motifs from Bub1/BubR1 family gene members. Two of these are novel ABBA motifs that flank KEN2 specifically in BubR1/Mad3-like proteins; we show that this highly conserved ABBA-KEN2-ABBA cassette is crucial for the SAC in human cells.

2. Results and discussion

2.1. Refined phylogenomic analysis of the MadBub gene family pinpoints 16 independent gene duplication events across the eukaryotic tree of life

To enable detailed reconstruction of subfunctionalization events of all known functional features after duplication of ancestral MadBub genes, we expanded our previously published set of homologues [24] through broader sampling of sequenced eukaryotic genomes, focusing on sequences closely associated with duplication events (electronic supplementary material, sequence file 1). Phylogenetic analyses of a multiple sequence alignment of the TPR domain (the only domain shared by all MadBub family members) of 149 MadBub homologues (electronic supplementary material, discussion and figure S1) corroborated the 10 independent duplications previously described [24] and allowed for a more precise determination of the age of the duplications. Strikingly, we found evidence for a number of additional independent duplications:

three duplications in stramenopile species of the SAR super group (Albuginaceae (#10 in figure 1*b*), *Ectocarpus siliculosis* (#11) and *Aureococcus anophagefferens* (#12)) and one at the base of basidiomycete fungi (puccinioimycetes (#4)). The BUBR1 paralogue in teleost fish underwent a duplication and fission event, of which the C-terminus product was retained only in the lineage leading to zebra fish (*Danio rerio* (#7)). Lastly, through addition of recently sequenced genomes we could specify a duplication around the time plants started to colonize land (bryophytes (#13)) and an independent duplication in the ancestor of higher plants (tracheophytes (#14)), followed by a duplication in the ancestor of the flowering plants (magnoliaphytes (#15)). These gave rise to three MadBub homologues, signifying additional subfunctionalization of the paralogues in the plant model organism *Arabidopsis thaliana*. It thus seems to be the case that such striking parallel subfunctionalization as we originally identified is indeed predictive for more of its occurrence in lineages whose genome sequences have since been elucidated.

2.2. De novo discovery, phylogenetic distribution and fate after duplication of functional motifs in the MadBub gene family

Previous analyses revealed a recurrent pattern of mutually exclusive retention of an N-terminal KEN-box and a C-terminal kinase domain after duplication of an ancestral MadBub gene [24,25]. These patterns suggested the hypothesis of paralogue subfunctionalization towards either inhibition of the APC/C in the cytosol (retaining the KEN-box) or attachment-error correction at the kinetochore (retaining the kinase domain). Given the extensive sequence divergence of MadBub homologues and a scala of different known functional elements, we reasoned that a comprehensive analysis of MadBub gene duplicates would provide opportunities for the discovery of novel and co-evolving ancestral features. For clarity, we refer to the Bub1-like paralogue (C-terminal kinase domain) as BUB and the BubR1/Mad3-like paralogue (N-terminal KEN-box) as MAD throughout the rest of this paper.

To capture conserved ancestral features of diverse eukaryotic MadBub homologues, we constructed a sensitive de novo motif and domain discovery pipeline (ConFeaX: conserved feature extraction) similar to our previous approach used to characterize KNL1 evolution [26]. In short, the MEME algorithm [27] was used to search for significantly similar gapless amino acid motifs, and extended motifs were aligned by MAFFT [28]. Alignments were modelled using HMMER [29] and sensitive profile HMM searches were iterated and specifically optimized using permissive *E*-values/bit scores until convergence (Material and methods and figure 1*a*). Owing to the degenerate nature of the detected SLiMs, we manually scrutinized the results for incorrectly identified features and supplemented known motif instances, when applicable. We preferred ConFeaX over other de novo motif discovery methods [30,31], as it does not rely on high quality full length alignment of protein sequences and allows detection of repeated or dynamic non-syntenic conserved features (which is a common feature for SLiMs). It is therefore better tuned to finding conserved features over long evolutionary distances in general and specifically in this case where recurrent
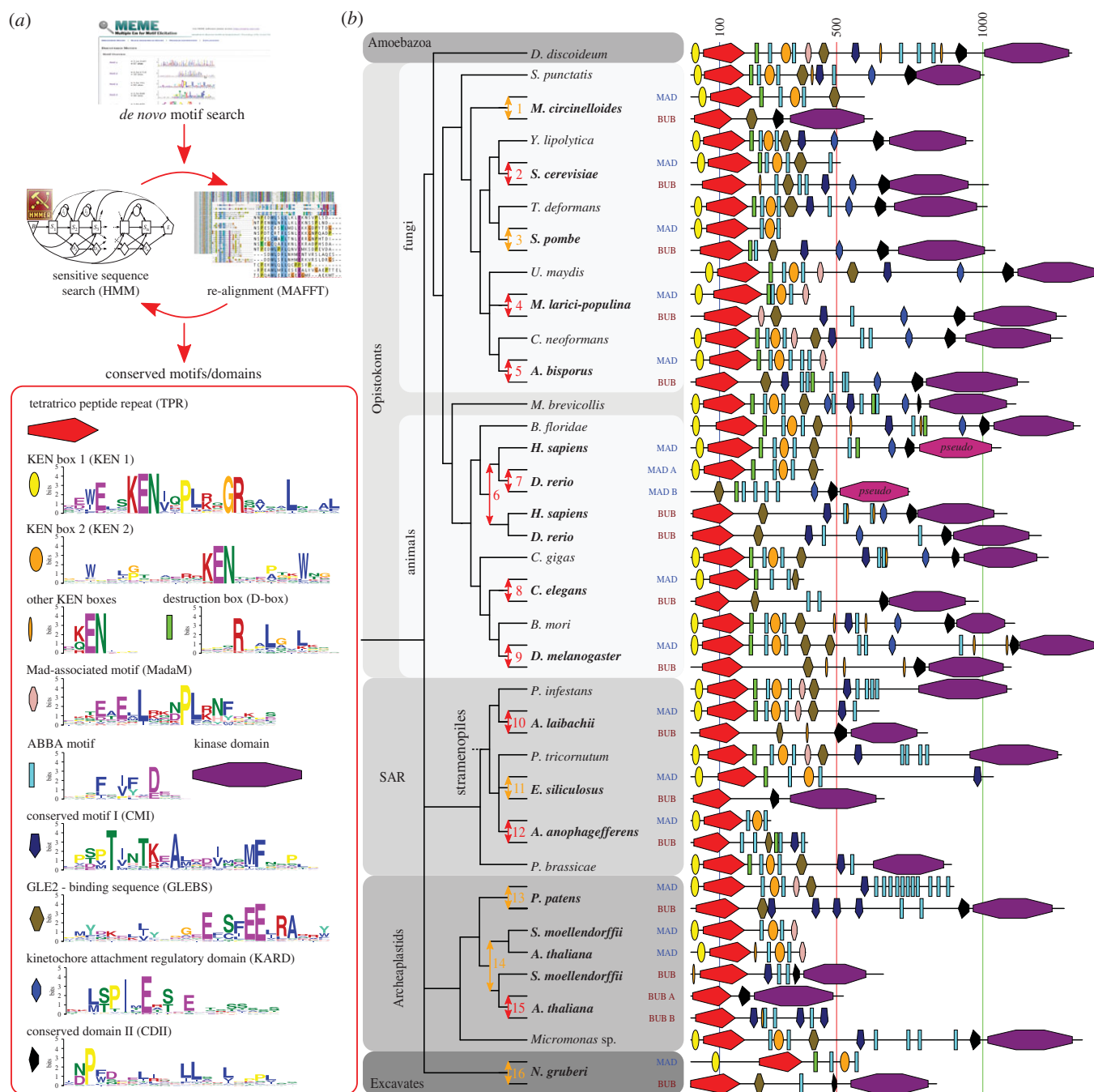
Figure 1. Fate of conserved functional sequence features after 16 independent duplications of the MADBUB gene family throughout eukaryotic evolution (*a*) Overview of the de novo sequence discovery pipeline ConFeaX including the ancestral conserved features of a search against the eukaryotic MADBUB gene family. The consensus sequences of the detected conserved motifs are depicted as a sequence logo (colours reflect distinct amino acid properties and height of the letters indicates conservation of amino acids). Each feature is assigned a differently coloured shape. (*b*) Cartoon of the evolutionary scenario of 16 independent duplications of the MADBUB gene family throughout eukaryotic evolution, including a projection of conserved features onto the linear protein representation (on scale). Gene duplications are indicated by an arrow (red: high confidence, orange: likely). The subfunctionalized paralogues MAD and BUB are coloured brown and blue, respectively. Numbers indicate the clades in which the duplications occurred: 1, Mucorales; 2, Saccharomycetaceae; 3, schizosaccharomycetes; 4, pucciniomycetes: 5, agaricomycetes (excluding early branching species); 6, vertebrates; 7, teleost fish; 8, nematodes; 9, diptera (flies); 10, Albuginaceae (oomycete); 11, Ectocarpales (brown algae); 12, *Aureococcus* (harmful algae bloom); 13, bryophytes (mosses); 14, tracheophytes (vascular plants); 15, magnoliaphytes (flowering plants); 16, *Naegleria*.

duplication and subfunctionalization hamper conventional multiple sequence alignment based analysis.

ConFeaX identified known functional motifs and domains and in some cases extended their definition: KEN1 [32], KEN2 [19], GLEBS [33], KARD [21–23], CMI (also known as CDI [7]), D-box [19], CDII (a co-activator domain of BUB1 [7,34]) and the recently discovered ABBA motif (termed ABBA3, see §2.3) [9,16,18,20] (figure 1*a*; electronic supplementary material, table SII and sequence file 2). The

TPR and the kinase domain were annotated using profile searches of previously established models [24] and excluded from de novo sequence searches. KEN1 and KEN2 could be discriminated by differentially conserved residues surrounding the core KEN-box (figure 1*a*). Those surrounding KEN1 are involved in the formation of the helix-turn-helix motif that positions BubR1/Mad3 towards Cdc20 [6], while two pseudo-symmetrically conserved tryptophan residues with unknown function specifically defined KEN2. Furthermore,

we found that the third position of the canonical ABBA motif is often occupied by a proline residue and the first position in ascomycetes (fungi) is often substituted for a polar amino acid (KRN) (figure 1a), signifying potential lineage-specific changes in Cdc20–ABBA interactions. Last, we also discovered a novel motif predominantly associated with the MAD paralogue in basidiomycetes, plants, amoeba and stramenopiles but not metazoa, which we termed MAD-associated motif (MadaM) (figure 1a).

Projection of the conserved ancestral features onto the MadBub gene phylogeny provided a highly detailed overview of MadBub motif evolution (figure 1b; electronic supplementary material, figure S1b). We found that the core functional motifs and domains (TPR, KEN1, KEN2, ABBA, D-box, GLEBS, MadaM, CMI, CDII and kinase) are present throughout the eukaryotic tree of life, representing the core features that were probably part of the SAC signalling network in the last eukaryotic common ancestor (LECA). Of note are lineages (nematodes, flatworms (*Schistosoma mansoni*), dinoflagellates (*Symbiodinium minutum*) and early branching fungi (microsporidia and *Conidiobolus coronatus*)) for which multiple features were either lost or considerably divergent (electronic supplementary material, figure S1b). Especially interesting is *Caenorhabditis elegans* in which both KEN boxes and the GLEBS domain appear to have been degenerated (ceMAD = san-1) and the CMI motif is lost (ceBUB = bub-1), indicating extensive rewiring or a less essential role of the SAC in nematode species, as has been suggested recently [35,36].

Our motif discovery analyses revealed the Cdc20/Cdh1-interacting ABBA motif to be much more abundant than the single instances that were previously reported for BUBR1 and BUB1 in humans [9,16,18]. We observed three different contexts for the ABBA motifs (figure 1b; electronic supplementary material, figure S1b): (i) in repeat arrays (e.g. MAD of *Physcomitrella patens*, basidiomycetes and stramenopiles), (ii) in the vicinity of CMI (many instances) and/or D-box/KEN (e.g. human) and (iii) as two highly conserved ABBA motifs flanking KEN2 (virtually all species). Because of the positional conservation of the latter, we have termed these ABBA1 and ABBA2. Any additional ABBA motifs were pooled in the category 'ABBA-other'.

In order to track the fate of the features discovered using ConFeaX, we quantified their co-presences and -absences, as a proxy for coevolution, by calculating the Pearson correlation coefficient (r) for the profiles of each domain/motif pair of 16 duplicated MadBub homologues (figure 1b) [37]. Subsequent average clustering of the Pearson distance ($d = 1 - r$) revealed two sets of co-segregating and anti-correlated conserved features (figure 2a,b) consistent with our hypothesis that MadBub gene duplication caused parallel subfunctionalization of features towards the kinetochore (mainly BUB) and the cytosol (MAD) [24]. GLEBS, CDI, ABBA-other, KARD, CDII and the kinase domain formed a coherent cluster of features with bona fide function at the kinetochore. For a detailed discussion on several intriguing observations regarding presence/absence of these motifs in several eukaryotic lineages, and what this may mean for BUB/MAD and SAC function in these lineages, see the electronic supplementary material, Discussion. A second cluster contained known motifs that bind and interact with (multiple) CDC20 molecules, including KEN1, KEN2 and (to a lesser extent) the D-box. Our newly discovered ABBA motifs that flank KEN2 were tightly associated with KEN2 and KEN1 (figure 2). As such, the ABBA1-KEN2-ABBA2 cassette (figure 3a) co-segregated with MAD function during subfunctionalization of MadBub gene duplicates. Although the D-box often co-occurs with the KEN–ABBA cluster, this motif was occasionally lost (e.g. archeaplastids, *Schizosaccharomyces pombe* and *A. anophagefferens*). Finally, MadaM co-segregated with the Cdc20-interacting motifs (figure 2a), suggesting a MAD-specific role for this newly discovered motif (possibly in MCC function and/or Cdc20-binding) in species harbouring it such as plants, basidiomycetes and stramenopiles.

2.3. The conserved ABBA1-KEN2-ABBA2 cassette is essential for SAC signalling in human cells

The strong correlation of the ABBA1-KEN2-ABBA2 cassette with KEN1 and the D-box urged us to examine the role of these motifs in BUBR1-dependent SAC signalling in human cells. We therefore generated stable isogenic HeLa-FlpIn cell lines expressing doxycyclin-inducible versions of LAP-tagged BUBR1 [38]. These included: ΔABBA1, ΔABBA2, ΔABBA1 + 2, alanine-substitutions of the two KEN2-flanking tryptophans (W1-A, W2-A and W1/2-A), KEN1-AAA, KEN2-AAA, ΔABBA3 and ΔD-box (figure 3a−c). The SAC was severely compromised in cells depleted of endogenous BUBR1 by RNAi, as measured by inability to maintain mitotic arrest upon treatment with S-trityl-L-cysteine (STLC) [39] (median (m) = 50 min from nuclear envelope breakdown to mitotic exit, compared with control ($m > 500$ min)) (figure 3d,e). SAC proficiency was restored by expression of siRNA-resistant LAP-BUBR1 ($m > 500$ min). As shown previously [19,40,41], mutants of KEN1, KEN2 and the D-box strongly affected the SAC. Importantly, BUBR1 lacking ABBA1 or ABBA2 or both, or either of the two tryptophans, could not rescue the SAC (figure 3e). We observed a consistently stronger phenotype for the mutated motifs on the N-terminal side of KEN2 (ΔABBA1 ($m = 65$ min) and W1-A ($m = 165$ min)) compared with those on the C-terminal side (ΔABBA2 ($m = 200$ min) and W2-A ($m = 260$ min)). The double ABBA (1/2) and tryptophan (1/2) mutants were however further compromised ($m = 50$ and 110 min, respectively), suggesting non-redundant functions. As expected from the interaction of ABBA motifs with the WD40 domain of CDC20 [14,18], BUBR1 lacking ABBA1 and/or ABBA2 was less efficient in binding APC/C-Cdc20 in mitotic human cells, to a similar extent as mutations in KEN1 (figure 3f). In our hands, the ABBA1 and ABBA2 mutants were strongly deficient in SAC signalling and APC/C-Cdc20 binding while the previously described ABBA motif (ABBA3) was not (figure 3d,e). Previous studies suggested that ABBA3 might play a role in SAC silencing [16,42], which raises the possibility that ABBA3 may somehow counteract binding of ABBA1 and/or ABBA2 to CDC20. In conclusion, the ABBA1-KEN2-ABBA2 cassette in BUBR1 is essential for APC/C inhibition by the SAC.

We here discovered a symmetric cassette of SLiMs containing two Cdc20-binding ABBA motifs and KEN2. This cassette strongly co-occurs with KEN1 in MAD-like and MadBub proteins throughout eukaryotic evolution and has important contributions to the SAC in human cells. Our co-precipitation experiments along with the known roles for ABBA-like motifs and KEN2 and their recent modelling into the MCC-APC/C structure [14,15] strongly suggest that the ABBA1-W-KEN2-W-ABBA2 cassette interacts with one or multiple Cdc20 molecules. Together with KEN1, these interactions probably
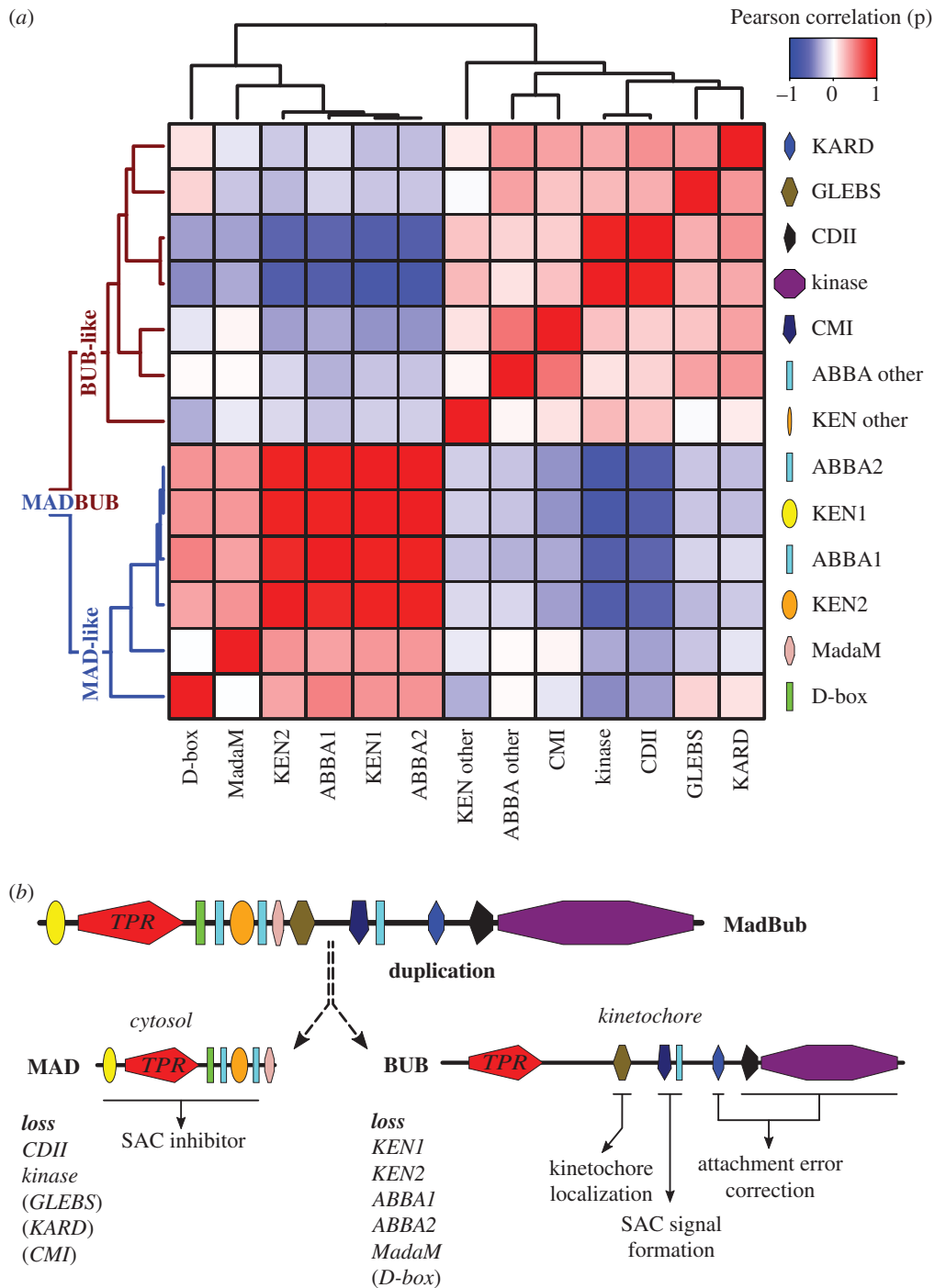
Figure 2. Coevolution of conserved features signify subfunctionalization of MAD and BUB after MADBUB duplication. (*a*) Average clustering based on Pearson distances of conserved ancestral feature correlation matrix (distance = 1 − *r*) of all MADBUB paralogues from figure 1. Red and blue indicate co-presence or -absence of features in the same paralogue, respectively. (*b*) Evolutionary scenario of MADBUB subfunctionalization: MAD (cytosol) as a SAC effector and BUB (kinetochore) involved in SAC signal formation and kinetochore microtubule attachment.

regulate affinity of MCC for APC/C or its positioning once bound to APC/C. The constellation of interactions between two Cdc20 molecules (Cdc20^{MCC} and Cdc20$^{APC/C}$) and the various Cdc20-binding motifs in one molecule of BUBR1 (3× ABBA, 2× KEN and a D-box) is not immediately clear, and will have to await detailed atomic insights. One suggestion that arises from our study is that the ABBA3 motif that is modelled into the APC/C-MCC structure by Alfieri *et al.* [14] might well be the ABBA2 motif. The symmetric arrangement of the cassette may be significant in this regard, as is the observation that (despite a highly conserved WD40 structure of Cdc20) the length of spacing between the ABBA motifs and KEN2 is highly variable between species. A more

detailed understanding of SAC function may be aided by Con-FeaX-driven discovery of lineage-specific conserved features in the MadBub family when more genome sequences become available, as well as of features in other SAC proteins families.

3. Material and methods

3.1. Phylogenomic analysis

We performed iterated sensitive homology searches with jackhmmer [43] (based on the TPR, kinase, CMI, GLEBS and KEN boxes) using a permissive *E*-value and bitscore cut-off to
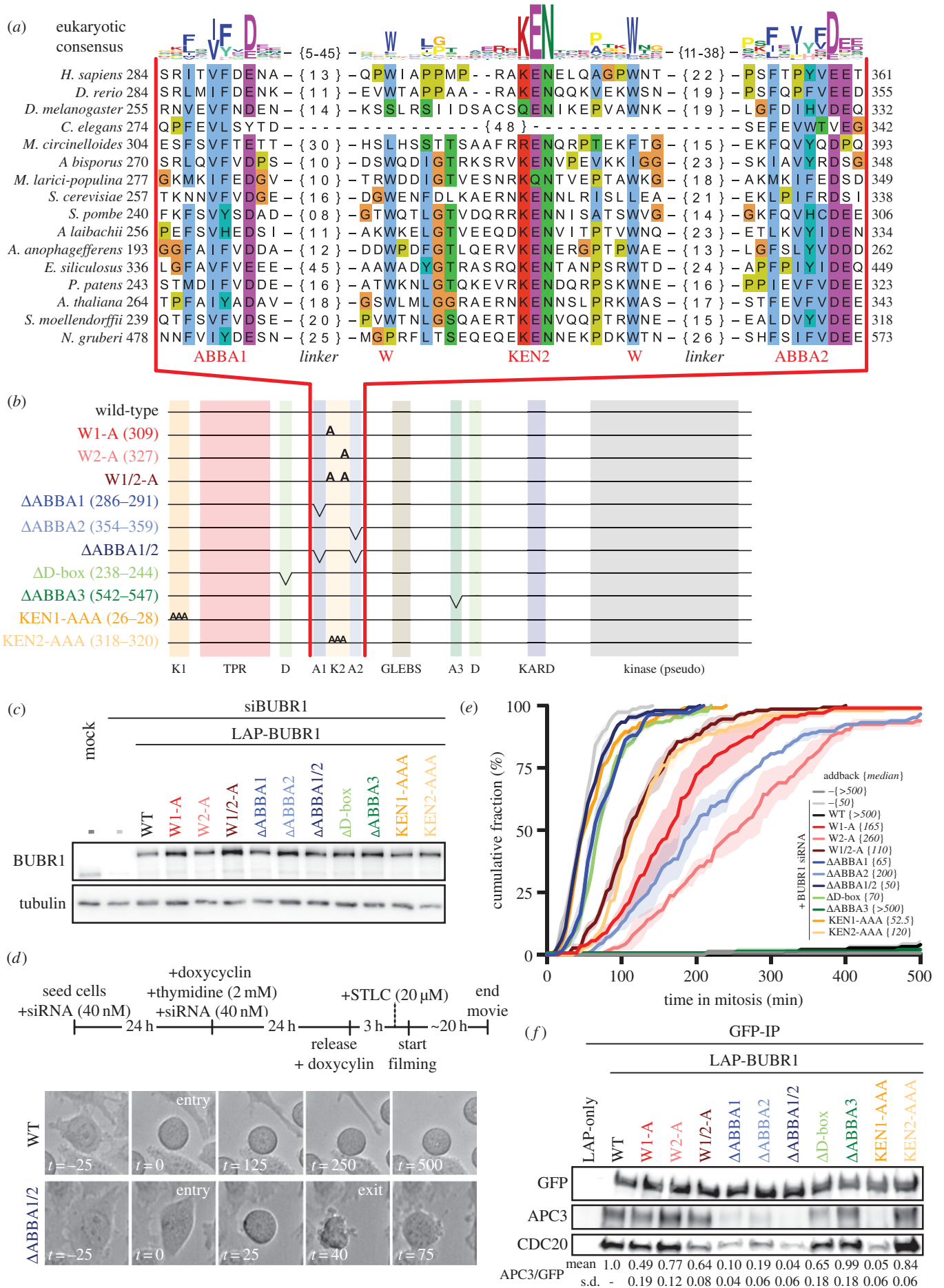
Figure 3. (*Caption overleaf.*)

Figure 3. (*Overleaf.*) The evolutionary conserved cassette ABBA1-KEN2-ABBA2 in BUBR1 is essential for SAC signalling. (*a*) Alignment of ABBA1-KEN2-ABBA2 cassette (red). Linkers (black) between ABBA motifs and KEN2 are indicated by {n}. The sequence logo on top is representative for all eukaryotic sequences (colours reflect distinct amino acid properties and height of the letters indicates conservation of amino acids). (*b*) Schematic representation of LAP-hBUBR1 mutants. Colour coding is consistent for each mutant in this figure. (*c*) Immunoblots of BUBR1 and tubulin of mitotic lysates of HeLa-FlpIn cell lines stably expressing LAP-tagged BUBR1 proteins. Cells were treated with siRNA (40 nM) for 48 h and cells were released and arrested into Taxol after double thymidine block. (*e*) Time-lapse analysis of HeLa-FlpIn cells expressing hBUBR1 mutants, treated with 20 μM STLC. Data ($N = 3$ with $n = 50$ per experiment) indicate the mean of cumulative fraction of cells that exit mitosis after nuclear envelope breakdown. Transparent regions represent the standard error of the mean. Values between braces {} indicate the median value. Cells were scored by cell morphology using DIC imaging; see (*d*) for examples of SAC deficient (ΔABBA1/2) and proficient cells (wild-type). Only YFP-positive cells were considered for analyses. (*f*) Immunoblots of GFP, APC3 and CDC20 in LAP-BUBR1 precipitations (LAP-pulldown) in whole cell lysates of mitotic HeLa-FlpIn cells expressing LAP-BUBR1 mutant constructs. The mean and standard deviation values of three independent APC3/GFP co-immunoprecipitation experiments for all mutant LAP-BUBR1 cell lines are normalized to wild-type LAP-BUBR1 and depicted below the immunoblots.

include diverged homologues on UniProt release 2016_08 and Ensemble Genomes 32 (http://www.ebi.ac.uk/Tools/hmmer/search/jackhmmer). Incompletely predicted genes were searched against whole genome shotgun contigs (wgs, http://www.ncbi.nlm.nih.gov/genbank/wgs) using tblastn. Significant hits were manually predicted using AUGUST [44] and GENESCAN [45]. In total, we used 152 MadBub homologues (electronic supplementary material, sequence file 1). The TPR domains of 148 sequences were aligned using MAFFT-LINSI [28]; only columns with 80% occupancy were considered for further analysis. Phylogenetic analysis of the resulting multiple sequence alignment was performed using RAxML [46] (electronic supplementary material, figure 1*a*). Model selection was performed using Prot Test [47] (Akaike information criterion): LG + G was chosen as the evolutionary model.

3.2. Conserved feature extraction and subfunctionalization analysis

ConFeaX starts with a probabilistic search for short conserved regions (max. 50) using the MEME algorithm (option: any number of repeats) [27]. Significant motif hits are extended on both sides by five residues to compensate for the strict treatment of alignment information by the MEME algorithm. Next, MAFFT-LINSI [28] introduces gaps and the alignments are modelled using the HMMER package [29] and used to search for hits that are missed by the MEME algorithm. Subsequent alignment and HMM searches were iterated until convergence. For SLiMs with few conserved positions, specific optimization of the alignments and HMM models using permissive E-values/bit scores was needed (e.g. ABBA motif and D-box). Sequence logos were obtained using weblogo2 [48]. Subsequently, from each of the conserved features, a phylogenetic profile was derived (present is '1' and absent is '0') for all duplicated MadBub sequences as presented in figure 1. For all possible pairs, we determined the correlation using Pearson correlation coefficient [37]. Average clustering based on Pearson distances ($d = 1 - r$) was used to indicate subfunctionalization.

3.3. Cell culture, transfection and plasmids

HeLa-FlpIn TRex cells were grown in DMEM high glucose supplemented with 10% Tet-free FBS (Clontech), penicillin/streptomycin (50 mg ml^{-1}) and alanyl-glutamine (Sigma; 2 mM). pCDNA5-constructs were co-transfected with pOgg44 recombinase in a 10 : 1 ratio [7] using FuGEHE HD (Roche) as a transfection reagent. After transfection, the medium was supplemented with puromycin (1 μg ml^{-1}) and blasticidin (8 μg ml^{-1}) until cells were fully confluent in a 10 cm culture dish. siBUBR1 (5′-AGAUCCUGGCUAACUGUUCUU-3′ custom Dharmacon) was transfected using Hiperfect (Qiagen) at 40 nM for 48 h according to the manufacturer's guidelines. RNAi-resistant LAP (YFP)-BUBR1 was subcloned from plC58 [38] into pCDNA5.1-puro using AflII and BamHI restriction sites. To acquire mutants, site-directed mutagenesis was performed using the quickchange strategy (for primer sequences see the electronic supplementary material, table SIII).

3.4. Live cell imaging

For live cell imaging experiments, the stable HeLa-FlpIn-TRex cells were transfected with 40 nM siRNA (start and at 24 h). After 24 h, the medium was supplemented with thymidine (2.5 mM) and doxycyclin (2 μg ml^{-1}) for 24 h to arrest cells in early S-phase and to induce expression of the stably integrated construct, respectively. After 48 h, cells were released for 3 h and arrested in prometaphase of the mitotic cell cycle (after approximately 8–10 h) by the addition of the Eg5 inhibitor S-trityl-L-cysteine (STLC, 20 μM). HeLa cells were imaged (DIC) in a heated chamber (37°C, 5% CO$_2$) using a CFI S Plan Fluor ELWD 20x/NA 0.45 dry objective on a Nikon Ti-Eclipse wide field microscope controlled by NIS software (Nikon). Images were acquired using an Andor Zyla 4.2 sCMOS camera and processed using NIS software (Nikon) and ImageJ.

3.5. Immunoprecipitation and western blot

HeLa-FlpIn-TRex cells were induced with doxycyclin (2 μg ml^{-1}) 48 h before harvesting. Synchronization by thymidine (2 mM) for 24 h and release for 10 h into Taxol (2 μM) arrested cells in prometaphase. Cells were collected by mitotic shake-off. Lysis was done in 50 mM Tris-HCl (pH 7.5), 100 mM NaCl, 0.5% NP40, 1 mM EDTA, 1 mM DTT, protease inhibitor cocktail (Roche) and phosphatase inhibitor cocktails 2 and 3 (Sigma). Complexes were purified using GFP-Trap beads (ChromoTek) for 15 min at 4°C. Precipitated proteins were washed with lysis buffer and eluted in 5× SDS sample buffer. Primary antibodies were used at the following dilutions for western blotting: BUBR1 (A300-386A, Bethyl) 1 : 2000, alpha-tubulin (T9026, Sigma) 1 : 5000, GFP (Custom) 1 : 10 000, APC1 (A301-653A, Bethyl) 1 : 2500, APC3 (gift from Phil Hieter) 1 : 2000, MAD2 (Custom) 1 : 2000, CDC20 (A301-180A, Bethyl) 1 : 1000. Western blot signals were detected by chemiluminescence using an ImageQuant LAS 4000 (GE Healthcare) imager.

References

1. Vleugel M, Hoogendoorn E, Snel B, Kops GJPL. 2012 Evolution and function of the mitotic checkpoint. *Dev. Cell* **23**, 239–250. (doi:10.1016/j.devcel.2012.06.013)

2. London N, Biggins S. 2014 Signalling dynamics in the spindle checkpoint response. *Nat. Rev. Mol. Cell Biol.* **15**, 736–747. (doi:10.1038/nrm3888)

3. Musacchio A. 2015 The molecular biology of spindle assembly checkpoint signaling dynamics. *Curr. Biol.* **25**, R1002–R1018. (doi:10.1016/j.cub.2015.08.051)

4. Sacristan C, Kops GJPL. 2015 Joined at the hip: kinetochores, microtubules, and spindle assembly checkpoint signaling. *Trends Cell Biol.* **25**, 21–28. (doi:10.1016/j.tcb.2014.08.006)

5. Izawa D, Pines J. 2014 The mitotic checkpoint complex binds a second CDC20 to inhibit active APC/C. *Nature* **517**, 631–634. (doi:10.1038/nature13911)

6. Chao WCH, Kulkarni K, Zhang Z, Kong EH, Barford D. 2012 Structure of the mitotic checkpoint complex. *Nature* **484**, 208–213. (doi:10.1038/nature10896)

7. Klebig C, Korinth D, Meraldi P. 2009 Bub1 regulates chromosome segregation in a kinetochore-independent manner. *J. Cell Biol.* **185**, 841–858. (doi:10.1083/jcb.200902128)

8. London N, Biggins S. 2014 Mad1 kinetochore recruitment by Mps1-mediated phosphorylation of Bub1 signals the spindle checkpoint. *Genes Dev.* **28**, 140–152. (doi:10.1101/gad.233700.113)

9. Vleugel M, Hoek TA, Tromer E, Sliedrecht T, Groenewold V, Omerzu M, Kops GJPL. 2015 Dissecting the roles of human BUB1 in the spindle assembly checkpoint. *J. Cell Sci.* **128**, 2975–2982. (doi:10.1242/jcs.169821)

10. Kawashima SA, Yamagishi Y, Honda T, Ishiguro K, Watanabe Y. 2010 Phosphorylation of H2A by Bub1 prevents chromosomal instability through localizing shugoshin. *Science* **327**, 172–177. (doi:10.1126/science.1180189)

11. Andrews PD, Ovechkina Y, Morrice N, Wagenbach M, Duncan K, Wordeman L, Swedlow JR. 2004 Aurora B regulates MCAK at the mitotic centromere. *Dev. Cell* **6**, 253–268. (doi:10.1016/S1534-5807(04)00025-5)

12. Tang Z, Bharadwaj R, Li B, Yu H. 2001 Mad2-independent inhibition of APC Cdc20 by the mitotic checkpoint protein BubR1. *Dev. Cell* **1**, 227–237. (doi:10.1016/S1534-5807(01)00019-3)

13. Sudakin V, Chan GKT, Yen TJ. 2001 Checkpoint inhibition of the APC/C in HeLa cells. *Cell* **154**, 925–936. (doi:10.1083/jcb.200102093)

14. Alfieri C, Chang L, Zhang Z, Yang J, Maslen S, Skehel M, Barford D. 2016 Molecular basis of APC/C regulation by the spindle assembly checkpoint. *Nature* **536**, 1–19. (doi:10.1038/nature19083)

15. Yamaguchi M et al. 2016 Cryo-EM of mitotic checkpoint complex-bound APC/C reveals reciprocal and conformational regulation of ubiquitin ligation. *Mol. Cell* **63**, 593–607. (doi:10.1016/j.molcel.2016.07.003)

16. Lischetti T, Zhang G, Sedgwick GG, Bolanos-Garcia VM, Nilsson J. 2014 The internal Cdc20 binding site in BubR1 facilitates both spindle assembly checkpoint signalling and silencing. *Nat. Commun.* **5**, 5563. (doi:10.1038/ncomms6563)

17. King EMJ, van der Sar SJA, Hardwick KG. 2007 Mad3 KEN boxes mediate both Cdc20 and Mad3 turnover, and are critical for the spindle checkpoint. *PLoS ONE* **2**, e342. (doi:10.1371/journal.pone.0000342)

18. DiFiore B, Davey N, Hagting A, Izawa D, Mansfeld J, Gibson T, Pines J. 2015 The ABBA motif binds APC/C activators and is shared by APC/C substrates and regulators. *Dev. Cell* **32**, 358–372. (doi:10.1016/j.devcel.2015.01.003)

19. Burton JL, Solomon MJ. 2007 Mad3p, a pseudosubstrate inhibitor of APCCdc20 in the spindle assembly checkpoint. *Genes Dev.* **21**, 655–667. (doi:10.1101/gad.1511107)

20. Davenport J, Harris LD, Goorha R. 2006 Spindle checkpoint function requires Mad2-dependent Cdc20 binding to the Mad3 homology domain of BubR1. *Exp. Cell Res.* **312**, 1831–1842. (doi:10.1016/j.yexcr.2006.02.018)

21. Suijkerbuijk SJE, Vleugel M, Teixeira A, Kops GJPL. 2012 Integration of kinase and phosphatase activities by BUBR1 ensures formation of stable kinetochore-microtubule attachments. *Dev. Cell* **23**, 745–755. (doi:10.1016/j.devcel.2012.09.005)

22. Kruse T, Zhang G, Larsen MSY, Lischetti T, Streicher W, Kragh Nielsen T, Bjørn SP, Nilsson J. 2013 Direct binding between BubR1 and B56-PP2A phosphatase complexes regulate mitotic progression. *J. Cell Sci.* **126**, 1086–1092. (doi:10.1242/jcs.122481)

23. Xu P, Raetz EA, Kitagawa M, Virshup DM, Lee SH. 2013 BUBR1 recruits PP2A via the B56 family of targeting subunits to promote chromosome congression. *Biol. Open* **2**, 479–486. (doi:10.1242/bio.20134051)

24. Suijkerbuijk SJE et al. 2012 The vertebrate mitotic checkpoint protein BUBR1 is an unusual pseudokinase. *Dev. Cell* **22**, 1321–1329. (doi:10.1016/j.devcel.2012.03.009)

25. Murray AW. 2012 Don't make me mad, Bub! *Dev. Cell* **22**, 1123–1125. (doi:10.1016/j.devcel.2012.05.020)

26. Tromer E, Snel B, Kops GJPL. 2015 Widespread recurrent patterns of rapid repeat evolution in the kinetochore scaffold KNL1. *Genome Biol. Evol.* **7**, 2383–2393. (doi:10.1093/gbe/evv140)

27. Bailey TL, Boden M, Buske FA, Frith M, Grant CE, Clementi L, Ren J, Li WW, Noble WS. 2009 MEME Suite: tools for motif discovery and searching. *Conflict* **37**, 202–208. (doi:10.1093/nar/gkp335)

28. Katoh K, Standley DM. 2013 MAFFT multiple sequence alignment software version 7: improvements in performance and usability. *Mol. Biol. Evol.* **30**, 772–780. (doi:10.1093/molbev/mst01)

29. Eddy SR. 2011 Accelerated profile HMM searches. *PLoS Comput. Biol.* **7**, e1002195. (doi:10.1371/journal.pcbi.1002195)

30. Davey NE, Cowan JL, Shields DC, Gibson TJ, Coldwell MJ, Edwards RJ. 2012 SLiMPrints: conservation-based discovery of functional motif fingerprints in intrinsically disordered protein regions. *Nucleic Acids Res.* **40**, 10 628–10 641. (doi:10.1093/nar/gks854)

31. Nguyen Ba AN, Yeh BJ, van Dyk D, Davidson AR, Andrews BJ, Weiss EL, Moses AM. 2012 Proteome-wide discovery of evolutionary conserved sequences in disordered regions. *Sci. Signal.* **5**, prs1. (doi:10.1126/scisignal.2002515)

32. Murray AW, Marks D. 2001 Can sequencing shed light on cell cycling? *Nature* **409**, 844–846. (doi:10.1038/35057033)

33. Taylor SS, Ha E, McKeon F. 1998 The human homologue of Bub3 is required for kinetochore localization of Bub1 and a Mad3/Bub1-related protein kinase. *J. Cell Biol.* **142**, 1–11. (doi:10.1083/jcb.142.1.1)

34. Kang J, Yang M, Li B, Qi W, Zhang C, Shokat KM, Tomchick DR, Machius M, Yu H. 2008 Structure and substrate recruitment of the human spindle checkpoint kinase Bub1. *Mol. Cell* **32**, 394–405. (doi:10.1016/j.molcel.2008.09.017)

35. Davey NE, Morgan DO. 2016 Building a regulatory network with short linear sequence motifs: lessons from the degrons of the anaphase-promoting complex. *Mol. Cell* **64**, 12–23. (doi:10.1016/j.molcel.2016.09.006)

36. Moyle MW, Kim T, Hattersley N, Espeut J, Cheerambathur DK, Oegema K, Desai A. 2014 A Bub1–Mad1 interaction targets the Mad1–Mad2

complex to unattached kinetochores to initiate the spindle checkpoint. *J. Cell Biol.* **204**, 647–657. (doi:10.1083/jcb.201311015)

37. Wu J, Kasif S, DeLisi C. 2003 Identification of functional links between genes using phylogenetic profiles. *Bioinformatics* **19**, 1524–1530. (doi:10.1093/BIOINFORMATICS/BTG187)

38. Suijkerbuijk SJE, Van Osch MHJ, Bos FL, Hanks S, Rahman N, Kops GJPL. 2010 Molecular causes for BUBR1 dysfunction in the human cancer predisposition syndrome mosaic variegated aneuploidy. *Cancer Res.* **70**, 4891–4900. (doi:10.1158/0008-5472.CAN-09-4319)

39. Ogo N, Oishi S, Matsuno K, Sawada J, Fujii N, Asai A. 2007 Synthesis and biological evaluation of L-cysteine derivatives as mitotic kinesin Eg5 inhibitors. *Bioorg. Med. Chem. Lett.* **17**, 3921–3924. (doi:10.1016/j.bmcl.2007.04.101)

40. Elowe S, Dulla K, Uldschmid A, Li X, Dou Z, Nigg EA. 2010 Uncoupling of the spindle-checkpoint and chromosome-congression functions of BubR1. *J. Cell Sci.* **123**, 84–94. (doi:10.1242/jcs.056507)

41. Lara-Gonzalez P, Scott MIF, Diez M, Sen O, Taylor SS. 2011 BubR1 blocks substrate recruitment to the APC/C in a KEN-box-dependent manner. *J. Cell Sci.* **124**, 4332–4345. (doi:10.1242/jcs.094763)

42. Diaz-Martinez LA, Tian W, Li B, Warrington R, Jia L, Brautigam CA, Luo X, Yu H. 2015 The Cdc20-binding Phe box of the spindle checkpoint protein BubR1 maintains the mitotic checkpoint complex during mitosis. *J. Biol. Chem.* **290**, 2431–2443. (doi:10.1074/jbc.M114.616490)

43. Finn RD, Clements J, Eddy SR. 2011 HMMER web server: interactive sequence similarity searching. *Nucleic Acids Res.* **39**, W29–W37. (doi:10.1093/nar/gkr367)

44. Stanke M, Tzvetkova A, Morgenstern B. 2006 AUGUSTUS at EGASP: using EST, protein and genomic alignments for improved gene prediction in the human genome. *Genome Biol.* **7**(Suppl 1), S11.1–S11.8. (doi:10.1186/gb-2006-7-s1-s11)

45. Burge C, Karlin S. 1997 Prediction of complete gene structures in human genomic DNA. *J. Mol. Biol.* **268**, 78–94. (doi:10.1006/jmbi.1997.0951)

46. Stamatakis A. 2014 RAxML version 8: a tool for phylogenetic analysis and post-analysis of large phylogenies. *Bioinformatics* **30**, 1312–1313. (doi:10.1093/bioinformatics/btu033)

47. Darriba D, Taboada GL, Doallo R, Posada D. 2011 ProtTest 3: fast selection of best-fit models of protein evolution. *Bioinformatics* **27**, 1164–1165. (doi:10.1093/bioinformatics/btr088)

48. Crooks GE, Hon G, Chandonia J-MM, Brenner SE. 2004 WebLogo: a sequence logo generator. *Genome Res.* **14**, 1188–1190. (doi:10.1101/gr.849004)